



1 **Tropospheric column ozone response to ENSO in GEOS-5**
2 **assimilation of OMI and MLS ozone data**

3

4 **Mark A. Olsen^{1,2}, Krzysztof Wargan^{3,4}, and Steven Pawson³**

5 ¹ Atmospheric Chemistry and Dynamics Laboratory, Code 614, NASA Goddard Space Flight
6 Center, Greenbelt, MD

7 ² Goddard Earth Science, Technology and Research Center, Morgan State University, Baltimore,
8 MD.

9 ³ Global Modeling and Assimilation Office, Code 610.1, NASA Goddard Space Flight Center,
10 Greenbelt, MD

11 ⁴ Science Systems and Applications Inc., Lanham, MD

12 Correspondence to: M. A. Olsen (mark.olsen@nasa.gov)

13

14 **Abstract**

15 We use GEOS-5 analyses of Ozone Monitoring Instrument (OMI) and Microwave Limb Sounder
16 (MLS) ozone observations to investigate the magnitude and spatial distribution of the El Niño
17 Southern Oscillation (ENSO) influence on tropospheric column ozone (TCO) into the middle
18 latitudes. This study provides the first explicit spatially resolved characterization of the ENSO
19 influence and demonstrates coherent patterns and teleconnections impacting the TCO in the
20 extratropics. The response is evaluated and characterized by both the variance explained and
21 sensitivity of TCO to the Niño 3.4 index. The tropospheric response in the tropics agrees well
22 with previous studies and verifies the analyses. However, we show a newly identified two-lobed
23 response symmetric about the Equator in the western Pacific/Indonesian region consistent with
24 the large-scale vertical transport. We also find that the large-scale transport in the tropics
25 dominates the response compared to the small-scale convective transport. The ozone response is
26 weaker in the middle latitudes, but significant explained variance of the TCO is found over
27 several small regions, including the central United States. However, the sensitivity of TCO to the



28 Niño 3.4 index is statistically significant over a large area of the middle latitudes. The sensitivity
29 maxima and minima coincide with anomalous anti-cyclonic and cyclonic circulations where the
30 associated vertical transport is consistent with the sign of the sensitivity. Also, ENSO related
31 changes to the mean tropopause height can contribute significantly to the midlatitude response.
32 Comparisons to a 22-year chemical transport model simulation demonstrate that these results
33 from the nine-year assimilation are representative of the longer-term. This investigation brings
34 insight to several seemingly disparate prior studies of the El Niño influence on tropospheric
35 ozone in the middle latitudes.

36

37 **1 Introduction**

38 The contributions by natural phenomena to tropospheric ozone variability must be identified and
39 quantified for robust assessments of the present and future anthropogenic influence. Here, we
40 investigate the signal of the El Niño Southern Oscillation (ENSO) in extratropical tropospheric
41 ozone in a global assimilation system. This study provides the first explicit spatially resolved
42 characterization of the ENSO influence, and reveals coherent patterns and mechanisms of the
43 influence in the extratropics.

44 ENSO is well known to impact the magnitude of tropospheric ozone in the tropical Pacific. El
45 Niño (La Niña) conditions are characterized by anomalous increases (decreases) in SSTs in the
46 central and eastern Pacific. Opposite anomalies tend to occur in the western Pacific. In general,
47 changes to convection and circulation patterns under El Niño conditions lead to reduced tropical
48 tropospheric ozone in the central and eastern Pacific and enhanced ozone over the western Pacific
49 and Indian Oceans. The response is highly linear in the tropics, so La Niña conditions produce an
50 antisymmetric response (DeWeaver and Nigam, 2002). This influence on tropical tropospheric
51 ozone has been observed in satellite data (e.g., Chandra et al., 1998; Thompson et al., 2001;
52 Ziemke et al., 2010; Ziemke et al., 2015) and ground-based measurements (e.g., Fujiwara et al.,
53 1999; Lee et al., 2010). Both chemical transport models (CTMs) driven by analyzed meteorology
54 and free-running models have simulated this impact of ENSO on the tropical ozone (e.g., Sudo
55 and Takahashi, 2001; Zeng and Pyle, 2005; Doherty et al., 2006; Oman et al., 2011).



56 The tropospheric ozone response to ENSO in the extratropics has not been as extensively studied
57 and some results from prior studies appear to be contradictory. ENSO events have been shown to
58 alter the extratropical circulation by modifying planetary wave driving, the North Pacific low, and
59 the location and strength of the extratropical jets (e.g., Angell and Korshover, 1984; Langford,
60 1999; Trenberth et al., 2002; García-Herrera et al., 2006). Thus, it is reasonable to expect ENSO
61 to have a dynamical impact on extratropical tropospheric ozone distribution and variability.
62 Oman et al. (2013) examined the ozone sensitivity to ENSO with Microwave Limb Sounder
63 (MLS) and Tropospheric Emission Spectrometer (TES) observations in addition to a chemical-
64 climate model simulation. Although limited by just over five years of TES data, they show
65 statistically significant sensitivity in the lower midlatitude troposphere over two broad meridional
66 bands centered on the Pacific and Indian Oceans. Balashov et al. (2014) and Thompson et al.
67 (2014) find a correlation between ENSO and tropospheric ozone around South Africa using air
68 quality monitoring station and ozonesonde data. Langford et al. (1998) and Langford (1999)
69 show ozone enhancements in the free troposphere correlated with ENSO (with a several month
70 lag) in lidar data from Boulder, CO. Langford (1999) attributes this to the secondary circulation
71 associated with an eastward shifted Pacific subtropical jet exit region under El Niño conditions.
72 The transverse circulation of ozone-rich air from the stratosphere across the jet is then transported
73 poleward. Lin et al. (2015) conclude that more frequent springtime stratospheric intrusions
74 following La Niña winters contribute to increased ozone at the surface and free troposphere in the
75 western United States.

76 In contrast, other observational and modeling studies have not found a significant relationship
77 between ENSO and extratropical tropospheric ozone, suggesting that any such influence is weak
78 or occurs only on a regional scale. For example, Vigouroux et al. (2015) use a stepwise multiple
79 regression model including an ENSO proxy to examine ground-based Fourier transform infrared
80 (FTIR) measurements from eight subtropical and extratropical stations of the Network for the
81 Detection of Atmospheric Composition Change (NDACC). They did not find a significant
82 ENSO impact on the tropospheric ozone column at any of the eight sites. Hess et al. (2015) also
83 did not find a relation between ENSO and tropospheric ozone over extratropical regions in a four-
84 member ensemble model simulation. They suggest that ENSO may occasionally induce ozone
85 anomalies but the correlation is weak.



86 Determining the spatial extent of ENSO influence on tropospheric ozone from observations is
87 difficult due to the sparse observation networks of sondes, FTIR, etc. The direct retrieval of
88 tropospheric ozone from satellite observations is limited by coarse vertical resolution in the
89 troposphere for nadir-viewing instruments and pressure broadening in the lower troposphere for
90 limb-type instruments. Nevertheless, sonde and surface data combined with satellite observations
91 have been used to derive a coarse global climatology of tropospheric ozone (Logan, 1999).
92 Tropospheric ozone fields have also been derived from subtracting measured stratospheric
93 column ozone from total column ozone (e.g., Fishman et al., 1990; Ziemke et al., 1998; Fishman
94 et al., 2003; Schoeberl et al., 2007). These residual methods are more robust at lower latitudes
95 and have been used to show a large impact by ENSO on tropospheric ozone in the tropics (e.g.,
96 Chandra et al., 1998; Ziemke et al., 1998; Thompson and Hudson, 1999; Ziemke and Chandra,
97 2003; Fishman et al., 2005).

98 The goal of this paper is to use NASA's Goddard Earth Observing System Version 5 (GEOS-5)
99 analyses of satellite measured ozone to investigate the spatial distribution, magnitude, and
100 attribution of the tropospheric ozone response to ENSO. Assimilation provides the advantages of
101 global, gridded fields constrained by observations. Ziemke et al. (2014) show that the ozone
102 assimilation offers more robust tropospheric ozone fields for science applications in the lower and
103 middle latitudes than residual methods. In the present study, the response in the tropics is
104 evaluated and discussed alongside the midlatitude response. The relatively well-established
105 tropical response is primarily included here for verification of the analyses, although several new
106 findings are discussed. The comprehensive examination of the midlatitudes made possible by the
107 ozone assimilation is novel to this study. In the midlatitudes, the tropospheric column ozone
108 (TCO) is found to have a statistically significant response to ENSO in some regions. This
109 response can be explained by changes to circulation, convection, and tropopause height. These
110 results will benefit both process-oriented evaluations of the regional ozone response in
111 simulations and assessments of the anthropogenic impact on tropospheric ozone, including
112 prediction of future tropospheric ozone and trends.

113 The following section discusses the data, assimilation system, and methods used in this study.
114 The results are then presented in Section 3. A comparison of results to a CTM simulation is
115 included to show that the nine-year time period of the EOS Aura observations is largely



116 representative of longer periods. Additional discussion of the results is found in Section 4 before
117 concluding with a brief summary.

118

119 **2 Data, assimilation system, and methods**

120 The ozone analyses used in this study were produced using a version of NASA's GEOS-5 data
121 assimilation system (DAS), ingesting data from the Ozone Monitoring Instrument (OMI) and
122 MLS on the Earth Observing System Aura satellite (EOS Aura), as described in Wargan et al.
123 (2015). A brief description of the ozone data and assimilation system is provided in the following
124 subsection. Subsequent subsections provide information on ancillary data sets used and the linear
125 regression analysis used in this study.

126 **2.1 Ozone data and GEOS-5 Data Assimilation System**

127 The OMI and MLS instruments are both onboard the polar orbiting EOS Aura satellite launched
128 on July 15, 2004. OMI is a nadir-viewing instrument that retrieves near-total column ozone
129 across a 60-scene swath perpendicular to the orbit (Levelt et al., 2006). The footprint, or spatial
130 resolution, of the nadir scene is 13 km along the orbital path by 24 km across the track. The
131 cross-track scene width increases with distance from nadir to about 180 km at the end rows. OMI
132 collection 3, version 8.5 retrieval algorithm data are used in the analyses considered here. The
133 MLS instrument scans the atmospheric limb to retrieve the ozone vertical profile from microwave
134 emissions. Version 3.3 data on the 38 layers between 261 hPa and 0.02 hPa were used in the
135 present analyses after screening based upon established guidelines (Livesey et al., 2011).

136 The GEOS-5.7.2 version of the data assimilation system is used to produce the ozone analyses.
137 This is a modified version from the system used in the Modern-Era Retrospective analysis for
138 Research and Applications (MERRA) (Rienecker et al., 2011). For the analyses used here, the
139 system uses a $2.5^{\circ} \times 2.0^{\circ}$ longitude-latitude grid with 72 layers from the surface to 0.01 hPa. The
140 vertical resolution around the tropopause is about 1 km. Alongside the ozone data, a large
141 number of in-situ and space-based observations are included in the GEOS-5 analyses (Wargan et
142 al., 2015). However, OMI and MLS ozone retrievals are the only data that directly modify the
143 analysis ozone in this version of the DAS. Anthropogenic and biomass burning ozone production



144 sources are not explicitly implemented in these analyses. However, some impact from emissions
145 and other tropospheric chemistry sources and sinks is included in the analyses to the extent that
146 each OMI column retrieval is sensitive to tropospheric altitudes (Wargan et al., 2015).

147 Wargan et al. (2015) and Ziemke et al. (2014) previously evaluated these ozone analyses relative
148 to sondes and other satellite data. Their assessments show that accounting for measurement and
149 model errors in the assimilation greatly increases the precision of the tropospheric ozone over
150 other methods of obtaining gridded TCO fields. Both Wargan et al. (2015) and Ziemke et al.
151 (2014) show that there is greater disagreement of the tropospheric ozone analyses with sondes at
152 high latitudes. For this reason, we restrict our discussion in the present study to the tropics and
153 middle latitudes.

154 **2.2 Global Modeling Initiative CTM simulation**

155 We use a Global Modeling Initiative (GMI) CTM (Strahan et al., 2007; Duncan et al., 2008)
156 simulation to determine if the results from the nine years of ozone analyses are representative of
157 the longer term. The simulation is driven using MERRA meteorological fields for 1991-2012
158 and run at the same resolution as the assimilation system. Observation-based, monthly-varying
159 surface emissions are used through 2010 with repeated 2010 monthly means for the final two
160 years. Strode et al. (2015) provide more details on this specific simulation, which they refer to as
161 the “standard hindcast simulation” in their study. Ziemke et al. (2014) show that the TCO from a
162 similar GMI simulation compares well with sonde observations. In the present study we define,
163 process, and analyze the CTM TCO fields in the same manner as the assimilation fields.

164 **2.3 ENSO index and outgoing longwave radiation data**

165 ENSO is characterized in this study by the monthly mean Niño 3.4 index available from the
166 NOAA Climate Prediction Center (<http://www.cpc.ncep.noaa.gov/data/indices/>). The index is
167 based upon the mean tropical sea surface temperature between 5° N – 5° S and 170° W – 120° W.
168 This time series is normalized using 1981-2010 as the base time period. Fig. 1 shows the index
169 time series from 1991-2013, which spans the years of the ozone analyses and GMI simulation. In
170 this study, we define “strong” El Niño and La Niña events as months with index values greater
171 than 0.75 and less than -0.75, respectively. The Climate Prediction Center uses threshold values



172 of 0.5 and -0.5 to characterize El Niño and La Niña, respectively. The values of ± 0.75 used here
173 to characterize “strong” events is about one standard deviation (0.78) of the time series spanning
174 the assimilation, 2005-2013. La Niña conditions were dominant during the ozone analyses time
175 period (black line in Fig. 1). Strong El Niño conditions occurred in the boreal fall/winter of
176 2006/2007 and 2009/2010. Strong La Niña conditions occurred during the boreal fall/winter of
177 2005/2006, 2007/2008, 2008/2009, 2010/2011, and 2011/2012.

178 We use outgoing longwave radiation (OLR) data as a proxy for convection to investigate the
179 contribution from changes in convection associated with ENSO. The monthly, $1^\circ \times 1^\circ$ data is
180 provided by the NOAA Earth System Research Laboratory (Lee, 2014). Small values of OLR
181 indicate substantial convection, and vice versa.

182 **2.4 Methods**

183 For the present study, we use the nine full years (2005-2013) of ozone analyses that have been
184 completed. To calculate the TCO, we define the tropopause at each grid point as the lower of the
185 380 K potential temperature and 3.5 potential vorticity unit ($1 \text{ PVU} = 10^{-6} \text{ m}^2 \text{ K kg}^{-1} \text{ s}^{-1}$) surfaces.
186 The daily TCO fields are smoothed horizontally by averaging each grid point with the eight
187 adjacent neighboring points. Monthly mean TCO is computed from the daily values. The large
188 seasonal variability in the TCO is removed at each point by subtracting the respective nine-year
189 mean for each month.

190 We use multiple linear regression of the TCO monthly mean time series onto the Niño 3.4 index
191 and the first four sine and cosine harmonics to evaluate the response of tropospheric ozone to
192 ENSO. That is, $TCO = \sum_i m_i X_i + \varepsilon$, where the X_i are the index and harmonic time series, m_i
193 are the best fit regression coefficients, and ε is the residual error. The regression is computed at
194 every model grid point. The F-test is used to compute the confidence level of the explained
195 variances (Draper and Smith, 1998). The calculated significance of the ozone sensitivity includes
196 the impact from any autocorrelation in the residual time series (Tiao et al., 1990). We find that
197 tests with time-lagged regressions from one to six months were generally no better than for zero-
198 lag regressions. Therefore, the results presented herein are computed with no lag of the ozone
199 time series. This is further discussed in section 4.



200

201 **3 Results**

202 In this section, we examine the magnitude, spatial distribution, and mechanisms of the TCO
203 response to ENSO. For reference, the multi-year annual mean TCO is shown in Fig. 2. The non-
204 seasonal variability is indicated by overlaid contours of one standard deviation of the
205 deseasonalized TCO expressed as a percent of the mean TCO. (Ziemke et al. (2014) illustrate the
206 large seasonal variability). The following two subsections present the explained variance and
207 TCO sensitivity to the Niño 3.4 index. Changes to advection and convection contributing to the
208 TCO response are examined in subsections 3.3 and 3.4. Subsection 3.5 evaluates the ENSO-
209 associated changes to the tropopause height and the impact on the TCO response. We conclude
210 this section with a comparison to CTM results in subsection 3.6 for the purpose of evaluating
211 how robust the results from nine years of ozone assimilation are compared to the longer term.

212 **3.1 Explained variance**

213 The percent variance of TCO explained by ENSO is shown in Fig. 3. The ENSO influence is
214 greatest in the tropical Pacific where the variance explained has a maximum of about 55%. This
215 well-known tropical response is associated with increased convection and upwelling in the central
216 and eastern Pacific during El Niño that lofts ozone-poor air into the mid- to upper-troposphere.
217 The anomalous warm ocean current that runs southward along the South American coast during
218 El Niño conditions (e.g., Trenberth, 1997) is evident in the tropospheric ozone response. A
219 northeastward tongue of relatively large magnitude also extends towards and across Central
220 America. An isolated significant maximum is also found between 20° N and 30° N in the
221 subtropical Pacific with explained variance of greater than 20%.

222 In the western Pacific and Indonesian region, ENSO is known to produce an opposite response to
223 the central and eastern Pacific due to increased upward transport during La Niña conditions. Two
224 lobes of significant explained variance of more than 20% are symmetric around the equator in
225 this region. Off the western coast of Australia, the southern lobe has a maximum of about 35%.

226 The impact by ENSO is less in the subtropics and middle latitudes compared to the tropical
227 Pacific. Still, the variance explained by ENSO is greater than 20% and statistically significant in



228 several isolated regions. Of particular note, the variance explained exceeds 25% over South
229 Africa and 20% over the central United States. These areas correspond to locations where
230 previous studies have found an ENSO signature in ground-based data (Balashov et al., 2014;
231 Thompson et al., 2014; Langford et al., 1998; Langford, 1999). The variance explained also
232 exceeds 20% in a small region south of New Zealand. Other midlatitude areas, such as the
233 northern Pacific and Atlantic, exceed 10% but are not statistically significant due to the length of
234 the time series.

235 **3.2 TCO sensitivity**

236 The sensitivity of TCO per degree change in the Niño 3.4 index is another measure of the ozone
237 response to ENSO determined by the regression analysis. The spatial distribution of the
238 sensitivity is shown in Fig. 4. Over the time period studied here, we find the response to be linear
239 with respect to the ENSO forcing. The large region of negative sensitivity in the central Pacific
240 corresponding to the maximum in explained variance is a result of the increased lofting of ozone-
241 poor air into the middle and upper troposphere under El Niño conditions. Thus, higher values of
242 the Niño 3.4 index correspond to decreases in the TCO. The opposite sensitivity is found in the
243 equatorial symmetric lobes over Indonesia and the eastern Indian Ocean where the increased
244 lofting (decreased TCO) occurs with La Niña (negative Niño 3.4 values). In the subtropics,
245 positive sensitivity is located between about 20° and 30° to the north and south of the large
246 central Pacific minimum. In addition, relatively strong negative sensitivity exists over South
247 Africa corresponding to the significant variance explained there. In the midlatitudes, a negative
248 albeit weaker response is seen over the United States. Statistically significant negative responses
249 are also found over the northern Pacific and Atlantic Oceans.

250 **3.3 Changes in advection**

251 The manner by which ENSO impacts the TCO is not well established by previous studies for
252 regions relatively far removed from the tropical Pacific ENSO oscillations of sea surface
253 temperatures. We examine the differences in circulation patterns for strong El Niño and La Niña
254 conditions to investigate the large-scale impact of the extratropical circulation relative to the
255 ozone sensitivity. The streamlines of the difference in the mean winds at 200 hPa for months



256 with Niño 3.4 index of greater than 0.75 and less than -0.75 are overlaid on the ozone sensitivity
257 contours in Fig. 4. In the Northern Hemisphere extratropics, anomalous cyclonic circulations
258 coincide with the regions of negative sensitivity over central Asia, the north Pacific, United
259 States, and the north Atlantic. The north Pacific and United States circulations agree well with
260 ENSO-associated upper-troposphere height anomalies observed by Mo and Livezey (1986) and
261 Trenberth et al. (1998). Similar cyclonic circulations aligned with negative sensitivity in the
262 Southern Hemisphere are seen over the southern Pacific Ocean and over the southern tip of South
263 America. Similarly, anomalous anticyclonic flow is associated with positive sensitivity over
264 much of the midlatitudes.

265 The meridional and vertical cross-section streamlines of the difference between the mean winds
266 between 180° W and 120° W for months with Niño 3.4 index greater and less than 0.75 and -0.75
267 respectively are shown in Fig. 5. The positive and negative sensitivity patterns in this region
268 shown in Fig. 4 coincide with the anomalous tropospheric downwelling and upwelling. In the
269 tropics, the anomalous upwelling lofts ozone-poor air into the mid- and upper-troposphere in
270 agreement with previous studies. Northward of about 40° N, the tropospheric upwelling
271 coincides with the cyclonic circulation and negative sensitivity shown in in Fig. 4. This is
272 consistent with increased upwelling induced by cyclonic circulation. Similarly, other anomalous
273 cyclonic circulations associated with negative sensitivity over North America, the north Atlantic,
274 and the southern tip of South America also correspond to regions of increased upwelling (not
275 shown). The positive sensitivity between about 15° N and 30° N corresponds with increased
276 downwelling and evidence of increased cross-jet transport from the stratosphere into the
277 troposphere in Fig. 5. Oman et al. (2013) find a similar positive sensitivity in this region and also
278 in the Southern Hemisphere subtropics in a GEOS-5 CCM simulation. In addition, Lin et al.
279 (2014) find that increases in springtime ozone following El Niño at the Mauna Loa Observatory
280 in Hawaii correspond to increased influence by Asian pollution. Here, the relative role of ozone-
281 rich pollution transport cannot be distinguished from the cross-jet transport since emissions are
282 not explicitly implemented in the assimilation. The extension of positive sensitivity contours
283 upstream into the western Pacific to Asia in Fig. 4 is consistent with an influence by Asian
284 emissions. However, El Niño and La Niña tend to peak in the Northern Hemisphere winter
285 months when the emissions are least, which would reduce the potential influence.



286 The qualitative interpretation of the upwelling and downwelling shown in Fig. 5 is supported by
287 comparison with the dynamical ozone tendency output by the assimilation system. Fig. 6 shows
288 the differences of the mean dynamical ozone tendencies averaged between 180° W and 120° W
289 for strong El Niño and La Niña months (the black line). The greatest differences occur in the mid
290 to upper troposphere, so the net ozone tendencies are shown for the region between the
291 tropopause and 350 hPa below the tropopause, which provides a constant mass comparison. In
292 the tropics, the El Niño – La Niña difference in the dynamical tendencies ranges between -0.2 to -
293 0.55 DU day⁻¹, consistent with greater upward transport of ozone-poor air during El Niño than La
294 Niña. In the lower extratropics, the dynamical tendency differences increase to around 0.2 DU
295 day⁻¹, corresponding with positive ENSO sensitivity in these regions and increased ozone during
296 El Niño. Negative values of about -0.1 DU day⁻¹ exist between 40° and 50° latitude that
297 correspond with negative sensitivity and upwelling. The small magnitudes at these latitudes are
298 about 1/6 of the maximum tropical magnitude, which is consistent with the ratio of the
299 sensitivities in these regions.

300 The positive sensitivity in the tropics around Indonesia corresponds with increased upwelling
301 during La Niña conditions rather than with El Niño. This is evident in the downward oriented
302 streamlines in Fig. 7 showing the circulation differences averaged between 85° E and 120° E for
303 strong El Niño – La Niña months. In the tropics, the magnitude of the difference is smallest near
304 the equator, resulting in the northern and southern tropical lobe structure of sensitivity maxima
305 seen in Fig. 4. The difference is greater in the Southern Hemisphere and the streamlines indicate
306 more stratosphere to troposphere transport than in the Northern Hemisphere as a possible reason
307 for the greater sensitivity in the southern lobe located around 15° S.

308 **3.4 Changes in convection**

309 In addition to the resolved advective vertical transport and stratosphere to troposphere transport,
310 TCO can also respond to ENSO through changes in the vertical transport due to convection and
311 mean depth of the tropospheric column (the tropopause height). This subsection examines the
312 potential impact from convection using differences in OLR as a proxy. Changes in the
313 tropopause height are presented in the following subsection.



314 The differences in the mean OLR for months with Niño 3.4 indices greater and less than 0.75 and
315 -0.75 over the nine years are shown in Fig. 8. The central Pacific is dominated by decreased OLR
316 by up to 25%, indicating greater convection under El Niño conditions. The maximum decrease is
317 displaced to the west of the extrema of explained variance and TCO sensitivity to ENSO (Fig. 3
318 and 4, respectively). Over the Indonesian region, the OLR is increased by up to 16%, indicating
319 reduced convection. Here, the maximum OLR changes are offset to the east of the explained
320 variance and sensitivity extrema.

321 These spatial offsets suggest that much of the tropical TCO sensitivity to ENSO is realized
322 through the resolved advective transport. This is supported by the comparison of the analyses
323 convective and dynamical tendency differences. Fig. 6 compares the El Niño – La Niña
324 differences in the analysis mid to upper tropospheric convective ozone tendencies (red line) and
325 dynamical tendencies (black line) between 180° W and 120° W. In the tropics, the convective
326 tendency differences range from -0.15 to 0.1 DU day⁻¹. The dynamical tendency differences are
327 negative and the magnitudes are more than twice as great as the convective tendency differences.
328 In the middle latitude north Pacific between 40° N and 50° N, the magnitude of the El Niño – La
329 Niña convective ozone tendency difference is similar to the dynamical tendency differences (Fig.
330 6). Thus, the impact on the TCO sensitivity from the resolved transport and convection in this
331 region are comparable in contrast to the tropics where the resolved transport is dominant.

332 **3.5 Impact from tropopause height differences**

333 The sensitivity of the tropopause pressure to the Niño 3.4 index determined by regression
334 analysis is shown in Fig. 9. The response of the tropopause pressure is generally symmetric
335 about the equator over the Pacific Ocean. Under El Niño conditions, a slightly greater mean
336 tropopause pressure (decreased height and shorter tropospheric column) occurs in the extratropics
337 poleward of the climatological subtropical jet. Equatorward, decreased tropopause pressures
338 occur with El Niño, except in the western tropical Pacific where there is a small positive
339 response. The pattern of tropopause response in the Pacific is similar to the 200 hPa circulation
340 anomalies in Fig. 4. The offset of the tropical response extrema to the north and south of the
341 equatorial TCO response (Fig. 4) indicates that very little of the equatorial TCO response is
342 attributable to changes in the depth of the tropospheric column. The maxima TCO response



343 around 25° N and 25° S generally coincide with where the tropopause height response is zero.
344 This also suggests that the positive TCO response here may be impacted by increased
345 stratosphere to troposphere transport of ozone rich air across the subtropical jet.

346 Changes in the depth of the tropospheric column associated with ENSO have a greater impact on
347 the TCO sensitivity in the middle latitudes than in the tropics. Throughout much of the
348 midlatitudes, positive tropopause pressure sensitivity coincides with negative TCO sensitivity and
349 vice versa. Particularly noteworthy in the extratropical Northern Hemisphere are the positive
350 tropopause pressure sensitivity maxima over the northern Pacific, North America, northern
351 Atlantic, and Asia. The positive and negative tropopause sensitivity over extratropical South
352 America also aligns closely to the TCO response.

353 Both the changes in transport (including vertical advection, convection, and cross-tropopause
354 transport) and the tropopause height can impact the magnitude of TCO. We use regression
355 analysis of the mean tropospheric mixing ratio on the Niño 3.4 index to make a rough estimate of
356 the relative influences of transport and tropopause height changes. The mean mixing ratio is
357 directly sensitive to changes in the transport but not to the tropopause pressure. Note that the
358 mean mixing ratio also inherently includes any dependence from changes in chemistry that are
359 associated with ENSO (Sudo and Takahashi, 2001; Stevenson et al., 2005; Doherty et al., 2006).
360 If the response is assumed linear with respect to changes in transport/chemistry and tropospheric
361 column depth, the variances explained by the TCO and mean mixing ratio can provide a first
362 order estimate of the relative roles of these factors. For example, if the TCO explained variance
363 in a region is 25% and the mixing ratio explained variance is 20%, the tropopause height would
364 account for an estimated 1/5 of the TCO response.

365 The spatial pattern of the mean mixing ratio explained variance (not shown) is very similar to the
366 TCO regression (Fig. 3) in the both the tropics and midlatitudes. Throughout the tropics, the
367 magnitudes of the variance explained are nearly identical. Thus, changes in transport/chemistry
368 dominate the TCO response in this region. However, at middle latitudes the explained variance
369 of mean mixing ratio is frequently less than that of the TCO, so the tropopause height plays a
370 greater role. For the previously noted Northern Hemisphere negative sensitivity extrema, we
371 estimate the tropopause height accounts for about a 1/4 of the TCO response to ENSO over the
372 United States, 1/2 of the response over the North Pacific, and 2/3 of the North Atlantic



373 sensitivity. The tropopause height is responsible for about 1/5 of the negative sensitivity around
374 midlatitude South America. Also, only about 1/5 or less of the positive TCO response in the
375 subtropical Pacific around the climatological subtropical jets is attributable to changes in the
376 tropopause height.

377 **3.6 Representativeness of the 9-year assimilation time series**

378 We use the 22-year (1991-2012) GMI CTM simulation described in section 2.2 to show that the
379 results from the nine years of assimilation are representative of the longer-term TCO response to
380 ENSO. The percentage of the simulated TCO variance explained by ENSO during 2005-2012 is
381 shown in Fig. 10a for comparison with the assimilated ozone results over nearly the same time
382 period (i.e., Fig. 3). The spatial distribution of the simulated TCO response is very similar. The
383 maximum variance explained occurs in the central Pacific. The northeast and southeast split
384 towards Central and South America is evident, but the southern fork is not as prominent. In the
385 area of Indonesia, the simulated explained variance exhibits the same lobe-like structure
386 symmetric about the equator. The maximum over the subtropical Pacific and isolated maxima
387 over the United States and South Africa also agree well with the assimilated ozone results.

388 Regression analysis of the 22-year time span of the hindcast simulation reveals that much of the
389 TCO response determined from the nine years of assimilation is consistent with the longer-term
390 response (Fig. 10b). Use of the longer time series also increases the area in which the explained
391 variance is statistically different from zero, particularly in the middle latitudes. The shape and
392 magnitude of the tropical explained variance is similar to the results from the shorter time period.
393 Two differences are the reduced magnitude extending into the Northern Hemisphere Atlantic and
394 the slight equatorward shift in the location of the Southern Hemispheric lobe in the Indonesian
395 region. In the southern subtropical Pacific near 25° S, the maximum in variance explained is
396 more prominent. Conversely, the maximum in the northern subtropical Pacific is suppressed over
397 the longer-term. However, there remains an enhancement of greater than 15% explained variance
398 near 135° W between 15° N and 30° N that is consistent with the shift in the exit region of the
399 subtropical jet and the associated secondary circulation (Langford, 1999). In the extratropical
400 northern Pacific, corresponding to the location of negative sensitivity in Fig. 4, the explained
401 variance is 10%-15% and statistically significant. The signal over the United States and South



402 Africa persists in the 22-year regression at over 20% explained variance. Over midlatitude
403 Europe and Asia, the spatial pattern of the explained variance differs between the 22-year and 8-
404 year regression results. This may be indicative of the variability and trends of emissions being
405 much more dominant than the ENSO influence in this region.

406

407 **4 Discussion**

408 **4.1 Tropical response**

409 The tropical tropospheric ozone response to ENSO has been extensively studied in many previous
410 observational and model investigations. The tropical response in the OMI/MLS ozone analyses
411 agrees well with these prior investigations and verifies the analyses. However, most studies that
412 evaluate the spatial distribution of the response do not show a two-lobe structure in the western
413 Pacific/Indonesian region as seen in the present study (e.g., Ziemke and Chandra, 2003). We
414 note that this two-lobe structure is also suggested in the ozone sensitivity computed from
415 Tropospheric Emission Spectrometer (TES) data shown by Oman et al. (2013) in their Fig. 5a.
416 The symmetric response in this region is likewise well simulated by the GMI CTM driven by
417 assimilated meteorology (Fig. 10). However, the free-running GEOS-5 Chemistry Climate
418 Model simulation examined by Oman et al. (2013) produces a single, broad response centered on
419 the Equator (their Fig. 5b) where the vertical wind differences are consistent with the single,
420 centered response. This demonstrates that the ozone response is very sensitive to changes in the
421 advective transport that must be well simulated to reproduce the observed tropospheric response.

422 **4.2 Timing of the response**

423 As discussed in section 2, sensitivity tests of possible lags in the ozone response in the regression
424 analysis did not increase the correlation between the regressed ozone and Niño 3.4 index or
425 increase the explained variance. In general, the correlation and explained variance remain nearly
426 constant or decreasing with lag times of one or two months in the middle latitudes. The
427 correlations generally decrease rapidly with longer lag times. This lack of improved regressions
428 using longer lag times indicates that there is minimal impact from long-range transport, including
429 transport in the stratosphere that modulates lower stratospheric ozone concentrations and hence,



430 the magnitude of large-scale stratosphere to troposphere exchange of ozone. This is consistent
431 with previous studies that find little relation between ENSO and large-scale stratosphere-
432 troposphere exchange at midlatitudes (e.g., Hsu and Prather, 2009; Hess et al., 2015). In the
433 present study, the changes to transport and tropopause height contributing to the TCO response
434 act over shorter time scales and potentially impact the entire or large portions of the tropospheric
435 column.

436 **4.3 Regional aspects of the midlatitude response**

437 In the middle latitudes, the statistically significant variance explained by ENSO shown in this
438 study occurs over small-scale regions, so it is not surprising that some previous studies fail to find
439 an ENSO influence over large-scale regions or in many surface-based observations. For example,
440 there is no statistically significant explained variance over the midlatitude regions of Canada,
441 Central Europe, and Japan considered by Hess et al. (2015). These regions also remain
442 insignificant in the 22-year CTM simulation in the present study.

443 Conversely, Langford et al. (1998) demonstrate a correlation of ENSO with lidar observations of
444 ozone near Boulder, Colorado. This coincides with the location of significant explained variance
445 and negative sensitivity we show in Figs. 3 and 4. However, Langford et al. (1998) show a
446 positive correlation of mid-tropospheric ozone with the ENSO time series where the ozone signal
447 lags ENSO by a few months. The lidar ozone anomalies are correlated with the subtropical jet
448 exit region in the northeastern Pacific (Langford, 1999). He hypothesizes that transverse
449 circulation across the ENSO-shifted jet exit region brings stratospheric air into subtropical
450 tropical troposphere where it descends with the secondary circulation and is then transported
451 northward to the central United States. In the present study, the suggestion of increased localized
452 stratosphere-to-troposphere transport and subsequent downwelling in the northern subtropical
453 Pacific is supported by the meridional cross-section of the anomalous wind field (Fig. 5) and the
454 relatively large TCO response evident in the explained variance and sensitivity (Figs. 3 and 4). It
455 is possible that episodic events may bring anomalously high ozone air to the central United States
456 from the subtropics that can impact at least a portion of the tropospheric column. However, we
457 find that the immediate negative influence by the ENSO-driven vertical transport and tropopause
458 height changes is dominant when considering the entire tropospheric column.



459 The negative sensitivity over the United States is consistent with the results of Lin et al. (2015).
460 They conclude that more frequent springtime stratospheric intrusions following La Niña winters
461 contribute to increased ozone at the surface and free troposphere in the western United States.
462 Since the stratospheric intrusions are associated with enhanced stratosphere to troposphere
463 transport, this can significantly increase the TCO through an influx of ozone-rich air at lower
464 altitudes.

465 **4.4 South African region**

466 We find significant explained variance and sensitivity of TCO around subtropical South Africa.
467 This is consistent with previous findings. Blalshov et al. (2014) show a correlation of surface
468 observations of ozone with ENSO. They attribute this association to increased ozone formation
469 from anthropogenic emissions under warmer and drier conditions occurring with El Niño.
470 Thompson et al. (2014) remove the ENSO signal from southern Africa region ozonesonde data to
471 investigate middle tropospheric ozone trends.

472 Unlike most of the midlatitude TCO response, the processes that drive the TCO response in the
473 southern Africa region are not clear considering the mechanisms investigated in this study. A
474 meridional cross-section of the difference in the resolved advective winds averaged between 15°
475 E and 55° E for strong El Niño and La Niña months (not shown) does not indicate coherent
476 upwelling consistent with the negative sensitivity found there. Overall, there is weak anomalous
477 downward transport between about 5 km and 11 km in this region. The differences in OLR (Fig.
478 8) are also not consistent with unresolved convection as the source of the negative sensitivity.
479 The tropopause height sensitivity to ENSO in this region (Fig. 9) is positive and similar to the
480 spatial pattern of TCO sensitivity (Fig. 4) but is weak compared to the relatively strong TCO
481 response. Therefore, much of the TCO response may be due to ENSO-related changes in the
482 ozone chemistry that requires further investigation beyond the scope of this study.

483

484 **5 Summary**

485 The assimilation of OMI and MLS data enables this first comprehensive study of the TCO
486 response along with the ancillary information to interpret and explain the results. We have used



487 regression analysis of the TCO to provide an observationally-constrained evaluation of the
488 magnitude and spatial distribution of the ENSO impact on TCO throughout the middle latitudes.
489 Prior results of the TCO response outside the tropics have been contradictory and limited by the
490 spatial distribution and sparseness of available data. The present study is able to unify and explain
491 many aspects of the seemingly disparate findings reported by previous studies.

492 While the examination of the response in the tropics is included primarily for completeness and
493 verification of the analyses, two results in this region are novel to this study. We find that
494 changes in the large-scale transport dominate the changes in convective transport to produce the
495 TCO response throughout much of the tropics. We also show a two-lobe response in the region
496 around Indonesia that is symmetric about the Equator with maxima near 15° N and 15° S.

497 The midlatitude ozone response to ENSO is not as strong as in the tropics. However, the
498 explained variance is statistically significant over several small regions for the 9-year analysis,
499 such as over the United States and south of New Zealand. Other areas have an explained
500 variance of greater than 10% that the 22-year CTM simulation suggests would be statistically
501 significant with a longer observation period. These regions include the northern Pacific and
502 around midlatitude South America.

503 The TCO sensitivity to ENSO is relatively small but statistically significant over much of the
504 midlatitudes. These regions of negative (positive) sensitivity are coincident with anomalous
505 cyclonic (anticyclonic) circulation. The anomalous circulations are associated with upwelling
506 and downwelling that are consistent with the sign of sensitivity. In addition to the contribution
507 by transport, changes in the tropopause height can contribute substantially to the middle latitude
508 TCO response by altering the depth of the tropospheric column.

509 This study using analyses of OMI and MLS ozone provides the first explicit spatially resolved
510 characterization of the ENSO influence and demonstrates coherent patterns and teleconnections
511 impacting the TCO in the extratropics. Although relatively weak, the ENSO-driven variability
512 needs to be considered in investigations of midlatitude tropospheric ozone, particularly on
513 regional scales. The spatial variability of the TCO response indicates the ENSO influence is
514 likely statistically insignificant for hemispheric studies or over other broad areas. However, the
515 variance explained by ENSO can be 10% or greater over smaller regions like the United States,



516 midlatitude South America, and South Africa. Thus, it will be important in attributing the
517 sources of variability and trends in TCO, such as by human-related activity. These results are
518 potentially useful for evaluating the spatially dependent model response of TCO to ENSO
519 forcing. In the extratropics, the ENSO signal is convolved with large extratropical circulation
520 variability from other sources. Thus, additional factors may need to be considered when
521 evaluating the midlatitude response in free-running models, particularly in ensemble simulations.

522

523 **Acknowledgements**

524 The authors would like to thank Paul Newman, Jerry Ziemke, Luke Oman, Anne Douglass, and
525 Susan Strahan for helpful discussions. Funding for this research was provided by NASA's
526 Modeling, Analysis and Prediction Program and by NASA NNH12ZDA001N-ACMAP. The
527 assimilated data used in this study are available through the Aura Validation Data Center website:
528 <http://avdc.gsfc.nasa.gov>. Simulations and assimilation were done at NASA's Climate
529 Computing Service under awards from HPC. The Niño 3.4 index used in this study is available
530 from the NOAA Climate Prediction Center at <http://www.cpc.ncep.noaa.gov/data/indices/>. The
531 OLR data is provided by the NOAA/OAR/ESRL PSD, Boulder, Colorado, USA, from their web
532 site at <http://www.esrl.noaa.gov/psd/>.

533 **References**

- 534 Angell, J. K., and J. Korshover: Some long-term relations between equatorial sea-surface
535 temperature, the four centers of action and 700 mb flow, *J. Climate Appl. Meteor.*, 23,
536 1326-1332, doi:10.1175/1520-0450(1984)023<1326:SLTRBE>2.0.CO;2, 1984.
- 537 Balashov, N. V., A. M. Thompson, S. J. Piketh, and K. E. Langerman: Surface ozone variability
538 and trends over the South African Highveld from 1990 to 2007, *J. Geophys. Res. Atmos.*,
539 119, 4323-4342, doi:10.1002/2013JD020555, 2014.
- 540 Chandra, S., J. R. Ziemke, W. Min, and W. G. Read: Effects of 1997-1998 El Niño on
541 tropospheric ozone and water vapor, *Geophys. Res. Lett.*, 25, 3867-3870,
542 doi:10.1029/98GL02695, 1998.
- 543 DeWeaver, E., and S. Nigam: Linearity in ENSO's atmospheric response, *J. Climate*, 15, 2446-
544 2461, doi:10.1175/1520-0442(2002)015<2446:LIESAR>2.0.CO;2, 2002.
- 545 Doherty, R. M., D. S. Stevenson, C. E. Johnson, W. J. Collins, and M. G. Sanderson:
546 Tropospheric ozone and El Niño–Southern Oscillation: Influence of atmospheric dynamics,
547 biomass burning emissions, and future climate change, *J. Geophys. Res.*, 111,
548 10.1029/2005JD006849, 2006.
- 549 Draper, N. R., and H. Smith (1998), *Applied Regression Analysis*, John Wiley & Sons, Inc.,
550 Hoboken, NJ, USA.
- 551 Duncan, B. N., J. J. West, Y. Yoshida, A. M. Fiore, and J. R. Ziemke: The influence of European
552 pollution on ozone in the Near East and northern Africa, *Atmos. Chem. Phys.*, 8, 2267-
553 2283, doi:10.5194/acp-8-2267-2008, 2008.
- 554 Fishman, J., C. E. Watson, J. C. Larsen, and J. A. Logan: Distribution of tropospheric ozone
555 determined from satellite data, *J. Geophys. Res.*, 95, 3599, doi:10.1029/JD095iD04p03599,
556 1990.
- 557 Fishman, J., A. E. Wozniak, and J. K. Creilson: Global distribution of tropospheric ozone from
558 satellite measurements using the empirically corrected tropospheric ozone residual
559 technique: Identification of the regional aspects of air pollution, *Atmos. Chem. Phys.*, 3,
560 893-907, doi:10.5194/acp-3-893-2003, 2003.



- 561 Fishman, J., J. K. Creilson, A. E. Wozniak, and P. J. Crutzen: Interannual variability of
562 stratospheric and tropospheric ozone determined from satellite measurements, *J. Geophys.*
563 *Res.*, 110, 10.1029/2005JD005868, 2005.
- 564 Fujiwara, M., K. Kita, S. Kawakami, T. Ogawa, N. Komala, S. Saraspriya, and A. Suropto:
565 Tropospheric ozone enhancements during the Indonesian Forest Fire Events in 1994 and in
566 1997 as revealed by ground-based observations, *Geophys. Res. Lett.*, 26, 2417-2420,
567 doi:10.1029/1999GL900117, 1999.
- 568 García-Herrera, R., N. Calvo, R. R. Garcia, and M. A. Giorgetta: Propagation of ENSO
569 temperature signals into the middle atmosphere: A comparison of two general circulation
570 models and ERA-40 reanalysis data, *J. Geophys. Res.*, 111, 10.1029/2005JD006061, 2006.
- 571 Hess, P., D. Kinnison, and Q. Tang: Ensemble simulations of the role of the stratosphere in the
572 attribution of northern extratropical tropospheric ozone variability, *Atmos. Chem. Phys.*, 15,
573 2341-2365, doi:10.5194/acp-15-2341-2015, 2015.
- 574 Hsu, J., and M. J. Prather: Stratospheric variability and tropospheric ozone, *J. Geophys. Res.*,
575 114, 10.1029/2008JD010942, 2009.
- 576 Langford, A. O.: Stratosphere troposphere exchange at the subtropical jet: Contribution to the
577 tropospheric ozone budget at midlatitudes, *Geophys. Res. Lett.*, 26, 2449-2452,
578 doi:10.1029/1999GL900556/pdf, 1999.
- 579 Langford, A. O., T. J. O'Leary, C. D. Masters, K. C. Aikin, and M. H. Proffitt: Modulation of
580 middle and upper tropospheric ozone at northern midlatitudes by the El Niño/Southern
581 Oscillation, *Geophys. Res. Lett.*, 25, 2667-2670, 1998.
- 582 Lee, H.-T., 2014: Climate Algorithm Theoretical Basis Document (C-ATBD): Outgoing
583 Longwave Radiation (OLR) - Daily. NOAA's Climate Data Record (CDR) Program,
584 CDRP-ATBD-0526, 46 pp.
585 [http://www1.ncdc.noaa.gov/pub/data/sds/cdr/CDRs/Outgoing%20Longwave%20Radiation](http://www1.ncdc.noaa.gov/pub/data/sds/cdr/CDRs/Outgoing%20Longwave%20Radiation%20-%20Daily/AlgorithmDescription.pdf)
586 [%20-%20Daily/AlgorithmDescription.pdf](http://www1.ncdc.noaa.gov/pub/data/sds/cdr/CDRs/Outgoing%20Longwave%20Radiation%20-%20Daily/AlgorithmDescription.pdf).
- 587 Lee, S., D. M. Shelow, A. M. Thompson, and S. K. Miller: QBO and ENSO variability in
588 temperature and ozone from SHADOZ, 1998–2005, *J. Geophys. Res.*, 115,



- 589 doi:10.1029/2009JD013320, 2010.
- 590 Levelt, P. F., G. H. J. van den Oord, M. R. Dobber, A. Malkki, V. Huib, J. de Vries, P. Stammes,
591 J. O. V. Lundell, and H. Saari: The ozone monitoring instrument, *Geoscience and Remote*
592 *Sensing, IEEE Transactions on*, 44, 1093-1101, doi:10.1109/TGRS.2006.872333, 2006.
- 593 Lin, M., L. W. Horowitz, S. J. Oltmans, A. M. Fiore, and S. Fan: Tropospheric ozone trends at
594 Mauna Loa Observatory tied to decadal climate variability, *Nature Geosci.*, 7, 136-143,
595 doi:10.1038/NGEO2066, 2014.
- 596 Lin, M., A. M. Fiore, L. W. Horowitz, A. O. Langford, S. J. Oltmans, D. Tarasick, and H. E.
597 Reider: Climate variability modulates western US ozone air quality in spring via deep
598 stratospheric intrusions, *Nat. Commun.*, 67105, doi:10.1038/ncomms8105, 2015.
- 599 Liu, X., P. K. Bhartia, K. Chance, L. Froidevaux, R. J. D. Spurr, and T. P. Kurosu: Validation of
600 Ozone Monitoring Instrument (OMI) ozone profiles and stratospheric ozone columns with
601 Microwave Limb Sounder (MLS) measurements, *Atmos. Chem. Phys.*, 10, 2539-2549,
602 doi:10.5194/acp-10-2539-2010, 2010.
- 603 Liu, X., P. K. Bhartia, K. Chance, R. J. D. Spurr, and T. P. Kurosu: Ozone profile retrievals from
604 the Ozone Monitoring Instrument, *Atmos. Chem. Phys.*, 10, 2521-2537, doi:10.5194/acp-
605 10-2521-2010, 2010.
- 606 Logan, J. A., I. A. Megretskaya, A. J. Miller, G. C. Tiao, D. Choi, L. Zhang, R. S. Stolarski, G. J.
607 Labow, S. M. Hollandsworth, and G. E. Bodeker: Trends in the vertical distribution of
608 ozone: A comparison of two analyses of ozonesonde data, *J. Geophys. Res.*, 104, 26373-
609 26399, 1999.
- 610 Mo, K. C., and R. E. Livezey: Tropical-extratropical geopotential height teleconnections during
611 the Northern Hemisphere winter, *Mon. Wea. Rev.*, 114, 2488-2515, doi:10.1175/1520-
612 0493(1986)114<2488:TEGHTD>2.0.CO;2, 1986.
- 613 Oman, L. D., J. R. Ziemke, A. R. Douglass, D. W. Waugh, C. Lang, J. M. Rodriguez, and J. E.
614 Nielsen: The response of tropical tropospheric ozone to ENSO, *Geophys. Res. Lett.*, 38,
615 10.1029/2011GL047865, 2011.
- 616 Oman, L. D., A. R. Douglass, J. R. Ziemke, J. M. Rodriguez, D. W. Waugh, and J. E. Nielsen:



- 617 The ozone response to ENSO in Aura satellite measurements and a chemistry-climate
618 simulation, *J. Geophys. Res. Atmos.*, 118, 965-976, doi:10.1029/2012JD018546, 2013.
- 619 Rienecker, M. M., M. J. Suarez, R. Gelaro, R. Todling, J. Bacmeister, E. Liu, M. G. Bosilovich,
620 S. D. Schubert, L. Takacs, G.-K. Kim, S. Bloom, J. Chen, D. Collins, A. Conaty, A. da
621 Silva, W. Gu, J. Joiner, R. D. Koster, R. Lucchesi, A. Molod, T. Owens, S. Pawson, P.
622 Pegion, C. R. Redder, R. Reichle, F. R. Robertson, A. G. Ruddick, M. Sienkiewicz, and J.
623 Woollen: MERRA: NASA's Modern-Era Retrospective Analysis for Research and
624 Applications, *J. Climate*, 24, 3624-3648, doi:10.1175/JCLI-D-11-00015.1, 2011.
- 625 Schoeberl, M. R., J. R. Ziemke, B. Bojkov, N. Livesey, B. Duncan, S. Strahan, L. Froidevaux, S.
626 Kulawik, P. K. Bhartia, S. Chandra, P. F. Levelt, J. C. Witte, A. M. Thompson, E. Cuevas,
627 A. Redondas, D. W. Tarasick, J. Davies, G. Bodeker, G. Hansen, B. J. Johnson, S. J.
628 Oltmans, H. Vömel, M. Allaart, H. Kelder, M. Newchurch, S. Godin-Beekmann, G.
629 Ancellet, H. Claude, S. B. Andersen, E. Kyrö, M. Parrondos, M. Yela, G. Zablocki, D.
630 Moore, H. Dier, D. G. von, P., P. Viatte, R. Stübi, B. Calpini, P. Skrivankova, V. Dorokhov,
631 B. de, H., F. J. Schmidlin, G. Coetzee, M. Fujiwara, V. Thouret, F. Posny, G. Morris, J.
632 Merrill, C. P. Leong, G. Koenig-Langlo, and E. Joseph: A trajectory-based estimate of the
633 tropospheric ozone column using the residual method, *J. Geophys. Res.*, 112,
634 10.1029/2007JD008773, 2007.
- 635 Stajner, I., K. Wargan, S. Pawson, H. Hayashi, L.-P. Chang, R. C. Hudman, L. Froidevaux, N.
636 Livesey, P. F. Levelt, A. M. Thompson, D. W. Tarasick, R. Stübi, S. B. Andersen, M. Yela,
637 G. König-Langlo, F. J. Schmidlin, and J. C. Witte: Assimilated ozone from EOS-Aura:
638 Evaluation of the tropopause region and tropospheric columns, *J. Geophys. Res.*, 113,
639 10.1029/2007JD008863, 2008.
- 640 Stevenson, D., R. Doherty, M. Sanderson, C. Johnson, B. Collins, and D. Derwent: Impacts of
641 climate change and variability on tropospheric ozone and its precursors, *Faraday Discuss.*,
642 130, 41-57, doi:10.1039/B417412G, 2005.
- 643 Strahan, S. E., B. N. Duncan, and P. Hoor: Observationally derived transport diagnostics for the
644 lowermost stratosphere and their application to the GMI chemistry and transport model,
645 *Atmos. Chem. Phys.*, 7, 2435-2445, doi:10.5194/acp-7-2435-2007, 2007.



- 646 Strode, S. A., J. M. Rodriguez, J. A. Logan, O. R. Cooper, J. C. Witte, L. N. Lamsal, M. Damon,
647 B. Van Aartsen, S. D. Steenrod, and S. E. Strahan: Trends and variability in surface ozone
648 over the United States, *J. Geophys. Res. Atmos.*, 120, doi:10.1002/2014JD022784, 2015.
- 649 Sudo, K., and M. Takahashi: Simulation of tropospheric ozone changes during 1997–1998 El
650 Niño: Meteorological impact on tropospheric photochemistry, *Geophys. Res. Lett.*, 28,
651 4091-4094, doi:10.1029/2001GL013335, 2001.
- 652 Thompson, A. M., N. V. Balashov, J. C. Witte, J. G. R. Coetsee, V. Thouret, and F. Posny:
653 Tropospheric ozone increases over the southern Africa region: bellwether for rapid growth
654 in Southern Hemisphere pollution, *Atmos. Chem. Phys.*, 14, 9855-9869, 2014.
- 655 Thompson, A. M., J. C. Witte, R. D. Hudson, H. Guo, J. R. Herman, and M. Fujiwara: Tropical
656 Tropospheric Ozone and Biomass Burning, *Science*, 291, 2128-2132,
657 doi:10.1126/science.291.5511.2128, 2001.
- 658 Thompson, A. M., and R. D. Hudson: Tropical tropospheric ozone (TTO) maps from Nimbus 7
659 and Earth Probe TOMS by the modified-residual method: Evaluation with sondes, ENSO
660 signals, and trends from Atlantic regional time series, *J. Geophys. Res.*, 104, 26961-26975,
661 doi:10.1029/1999JD900470, 1999.
- 662 Tiao, G. C., G. C. Reinsel, D. Xu, J. H. Pedrick, X. Zhu, A. J. Miller, J. J. DeLuisi, C. L. Mateer,
663 and D. J. Wuebbles: Effects of autocorrelation and temporal sampling schemes on estimates
664 of trend and spatial correlation, *J. Geophys. Res.*, 95, 20507,
665 doi:10.1029/JD095iD12p20507, 1990.
- 666 Trenberth, K. E.: The Definition of El Niño, *Bull. Amer. Meteor. Soc.*, 78, 2771-2777,
667 doi:10.1175/1520-0477(1997)078<2771:TDOENO>2.0.CO;2, 1997.
- 668 Trenberth, K. E., G. W. Branstator, D. Karoly, A. Kumar, N.-C. Lau, and C. Ropelewski:
669 Progress during TOGA in understanding and modeling global teleconnections associated
670 with tropical sea surface temperatures, *J. Geophys. Res.*, 103, 14291-14324,
671 doi:10.1029/97JC01444, 1998.
- 672 Trenberth, K. E., J. M. Caron, D. P. Stepaniak, and S. Worley: Evolution of El Niño–Southern
673 Oscillation and global atmospheric surface temperatures, *J. Geophys. Res.*, 107,



- 674 10.1029/2000JD000298, 2002.
- 675 Vigouroux, C., T. Blumenstock, M. Coffey, Q. Errera, O. García, N. B. Jones, J. W. Hannigan, F.
676 Hase, B. Liley, E. Mahieu, J. Mellqvist, J. Notholt, M. Palm, G. Persson, M. Schneider, C.
677 Servais, D. Smale, L. Thölix, and M. De, M.: Trends of ozone total columns and vertical
678 distribution from FTIR observations at eight NDACC stations around the globe, Atmos.
679 Chem. Phys., 15, 2915-2933, doi:10.5194/acp-15-2915-2015, 2015.
- 680 Wargan, K., S. Pawson, M. A. Olsen, J. C. Witte, A. R. Douglass, J. R. Ziemke, S. E. Strahan,
681 and J. E. Nielsen: The global structure of upper troposphere-lower stratosphere ozone in
682 GEOS-5: A multiyear assimilation of EOS Aura data, J. Geophys. Res. Atmos., 120, 2013-
683 2036, doi:10.1002/2014JD022493, 2015.
- 684 Zeng, G., and J. A. Pyle: Influence of El Niño Southern Oscillation on stratosphere/troposphere
685 exchange and the global tropospheric ozone budget, Geophys. Res. Lett., 32,
686 10.1029/2004GL021353, 2005.
- 687 Ziemke, J. R., S. Chandra, and P. K. Bhartia: Two new methods for deriving tropospheric column
688 ozone from TOMS measurements: Assimilated UARS MLS/HALOE and convective-cloud
689 differential techniques, J. Geophys. Res., 103, 22115-22127, doi:10.1029/98JD01567, 1998.
- 690 Ziemke, J. R., S. Chandra, L. D. Oman, and P. K. Bhartia: A new ENSO index derived from
691 satellite measurements of column ozone, Atmos. Chem. Phys., 10, 3711-3721,
692 doi:10.5194/acp-10-3711-2010, 2010.
- 693 Ziemke, J. R., A. R. Douglass, L. D. Oman, S. E. Strahan, and B. N. Duncan: Tropospheric ozone
694 variability in the tropics from ENSO to MJO and shorter timescales, Atmos. Chem. Phys.,
695 15, 8037-8049, doi:10.5194/acp-15-8037-2015, 2015.
- 696 Ziemke, J. R., M. A. Olsen, J. C. Witte, A. R. Douglass, S. E. Strahan, K. Wargan, X. Liu, M. R.
697 Schoeberl, K. Yang, T. B. Kaplan, S. Pawson, B. N. Duncan, P. A. Newman, P. K. Bhartia,
698 and M. K. Heney: Assessment and applications of NASA ozone data products derived from
699 Aura OMI/MLS satellite measurements in context of the GMI chemical transport model, J.
700 Geophys. Res. Atmos., 119, 5671-5699, doi:10.1002/2013JD020914, 2014.
- 701 Ziemke, J. R., and S. Chandra: La Nina and El Nino induced variabilities of ozone in the tropical



702 lower atmosphere during 1970–2001, Geophys. Res. Lett., 30, 1142,
703 doi:10.1029/2002GL016387, 2003.
704



705 **Figure captions**

706 **Fig. 1.** Time series of the Niño 3.4 index (K) from 1991 through 2013. The time period of ozone
707 analyses is the black line (2005-2013). The red line indicates the additional years covered by the
708 GMI simulation. Dashed lines are +0.75 and -0.75 that are considered strong El Niño and La
709 Niña conditions in this study.

710 **Fig. 2.** The 2005-2013 annual mean TCO (color contours) from the analyses. Black contours
711 indicate one standard deviation of the deseasonalized TCO expressed as a percent of the annual
712 mean TCO. Black contour interval is 0.5%.

713 **Fig. 3.** The deseasonalized TCO variance explained by ENSO from the linear regression over
714 2005-2013. Crosshatched areas denote where the confidence level of the explained variance
715 being different from zero is less than 95%. The increment of the white contours is 5%.

716 **Fig. 4.** The TCO sensitivity to the Niño 3.4 index from the linear regression over 2005-2013
717 (color contours). The sensitivity is expressed as the change in the TCO per degree change in the
718 index (DU K^{-1}). Crosshatched regions denote where the sensitivity is not statistically different
719 from zero at the 95% confidence level. White contours are incremented every 0.3 DU K^{-1} . The
720 streamlines show the difference between the mean winds at 200 hPa for months with strong El
721 Niño conditions (Niño 3.4 index greater than 0.75) minus months of strong La Niña conditions
722 (Niño 3.4 index less than -0.75). The thickness of the streamlines is scaled to the magnitude of
723 the difference. Particularly note the midlatitude regions of negative and positive sensitivity
724 aligned with anomalous cyclonic and anticyclonic circulations, as discussed in the text.

725 **Fig. 5.** Streamlines of the difference between the mean vertical and meridional winds for months
726 with strong El Niño conditions minus months of strong La Niña conditions from 2005-2013. The
727 means are calculated between 180° W and 120° W . The width of the streamlines is proportional
728 to the magnitude of the difference. The dashed line indicates the mean tropopause pressure for
729 strong El Niño months. Solid contours are the zonal mean wind for strong El Niño months.

730 **Fig. 6.** The dynamical (black) and convective (red) ozone tendency differences between months
731 of strong El Niño and La Niña conditions from the assimilation system over 2005-2013. The
732 means are calculated between 180° W and 120° W , matching that of Fig. 5.

733 **Fig. 7.** As in Fig. 5, but averaged between 85° E and 120° E .



734 **Fig. 8.** Difference in the outgoing longwave radiation (OLR) for months with strong El Niño
735 conditions minus months of strong La Niña conditions from 2005-2013. The differences are
736 expressed as percent of annual mean OLR. Thin white lines are incremented every 2%.

737 **Fig. 9.** The sensitivity of tropopause pressure to the Niño 3.4 index from linear regression over
738 2005-2013. The sensitivity is expressed as the change in tropopause pressure per degree change
739 in the index (hPa K^{-1}). Crosshatched regions denote where the sensitivity is not statistically
740 different from zero at the 95% confidence level. White contours are incremented every 2 hPa K^{-1} .
741

742 **Fig. 10.** The deseasonalized TCO variance explained by ENSO in the GMI CTM simulation for
743 years (a) 2005-2012 and (b) 1991-2012. Crosshatched areas denote where the confidence level of
744 the explained variance being different from zero is less than 95%. The increment of the white
745 contours is 5%.

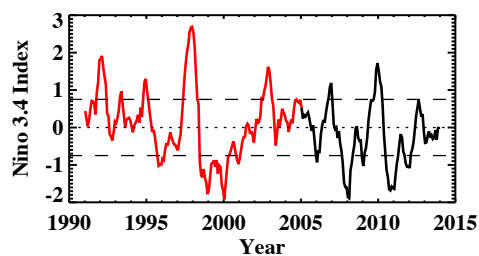


Figure 1. Time series of the Niño 3.4 index (K) from 1991 through 2013. The time period of ozone analyses is the black line (2005-2013). The red line spans the additional years covered by the GMI simulation. Dashed lines are +0.75 and -0.75 that are considered strong El Niño and La Niña conditions in this study.

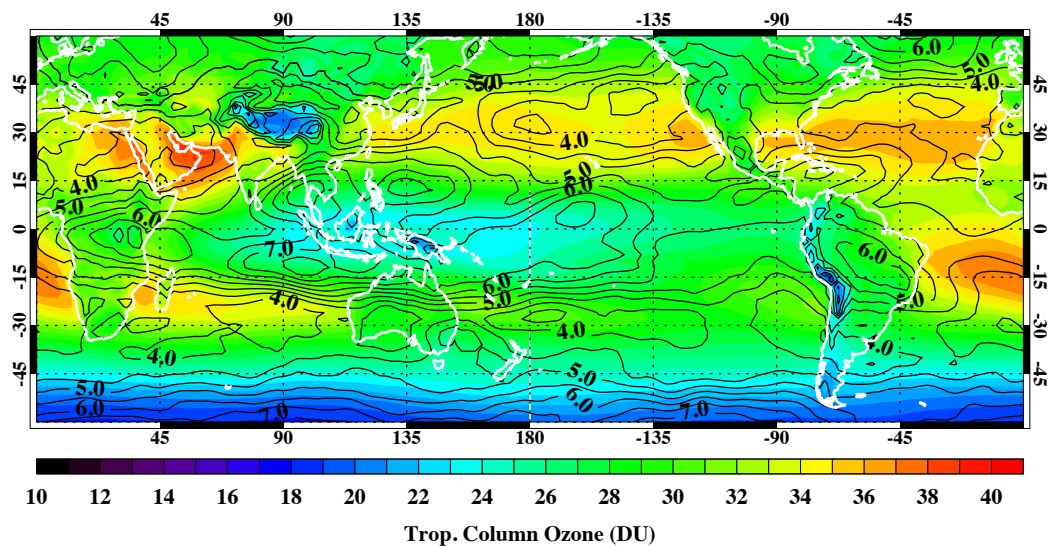


Figure 2. The 2005-2013 annual mean TCO (color contours) from the analyses. Black contours indicate one standard deviation of the deseasonalized TCO expressed as a percent of the annual mean TCO. Black contour interval is 0.5%.

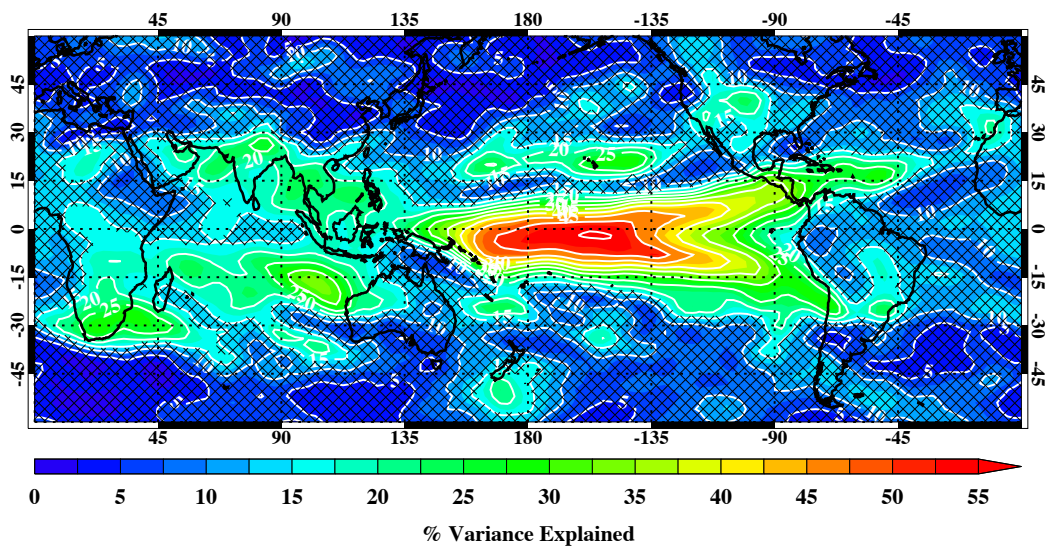


Figure 3. The deseasonalized TCO variance explained by ENSO from the linear regression over 2005-2013. Crosshatched areas denote where the confidence level of the explained variance being different from zero is less than 95%. The increment of the white contours is 5%.

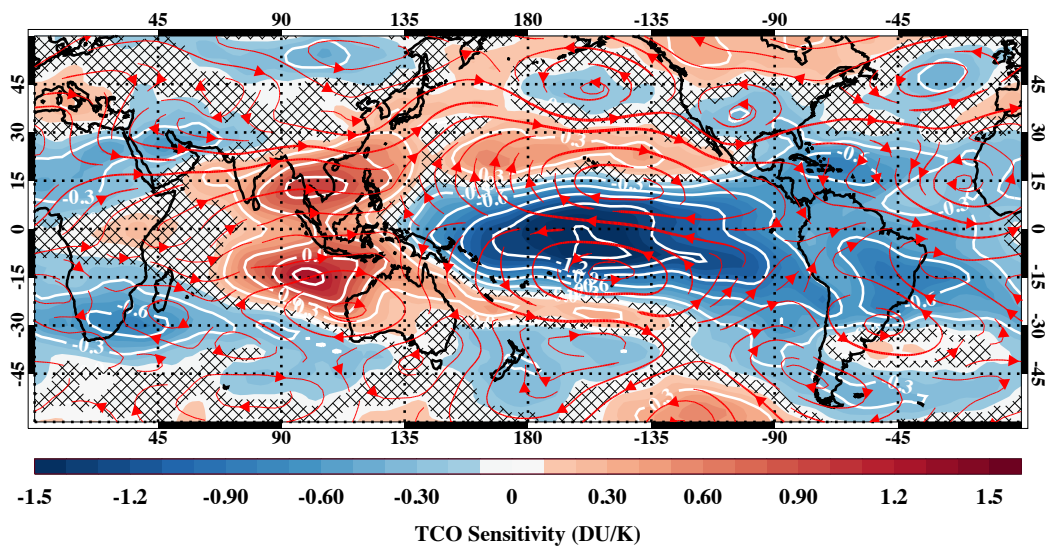


Figure 4. The TCO sensitivity to the Niño 3.4 index from the linear regression over 2005-2013 (color contours). The sensitivity is expressed as the change in the TCO per degree change in the index (DU/K). Crosshatched regions denote where the sensitivity is not statistically different from zero at the 95% confidence level. White contours are incremented every 0.3 DU/K. The streamlines show the difference between the mean winds at 200 hPa for months with strong El Niño conditions (Niño 3.4 index greater than 0.75) minus months of strong La Niña conditions (Niño 3.4 index less than -0.75). Particularly note the midlatitude regions of negative and positive sensitivity aligned with anomalous cyclonic and anticyclonic circulations, as discussed in the text.

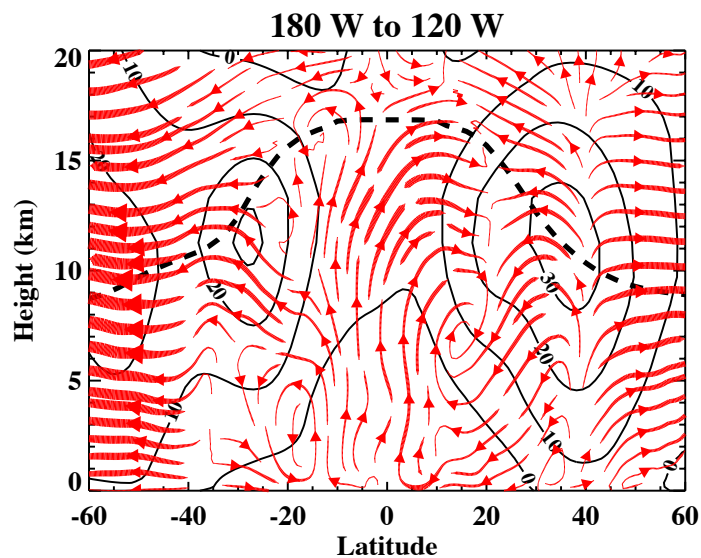


Figure 5. Streamlines of the difference between the mean vertical and meridional winds for months with strong El Niño conditions minus months of strong La Niña conditions from 2005-2013. The means are calculated between 180° W and 120° W. The width of the streamlines is proportional to the magnitude of the difference. The dashed line indicates the mean tropopause pressure for strong El Niño months. Solid contours are the zonal mean wind for extreme El Niño months.

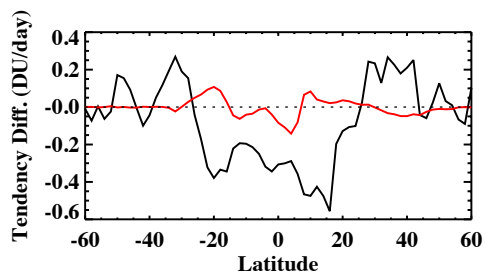


Figure 6. The dynamical (black) and convective (red) ozone tendency differences between months of strong El Niño and La Niña conditions from the assimilation system over 2005-2013. The means are calculated between 180° W and 120° W, matching that of Figure 4.

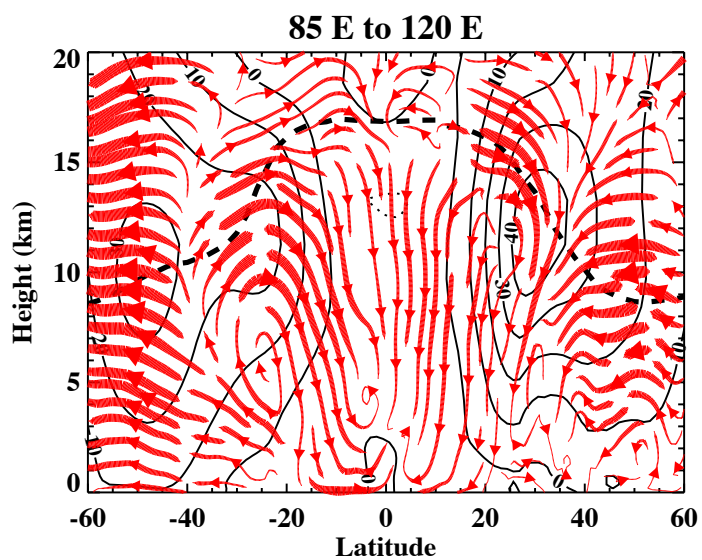


Figure 7. As in Figure 4, but averaged between 85° E and 120° E.

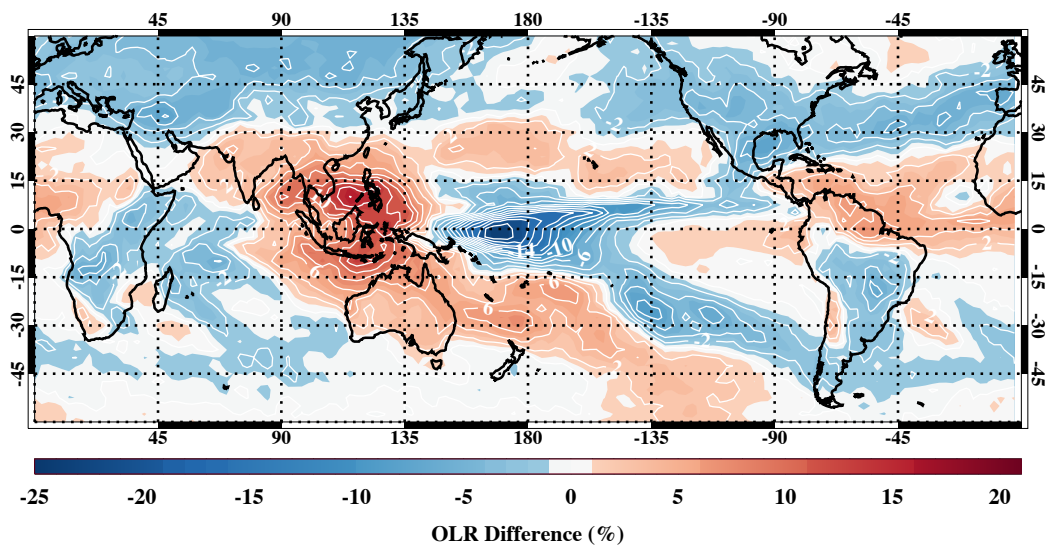


Figure 8. Difference in the outgoing longwave radiation (OLR) for months with strong El Niño conditions minus months of strong La Niña conditions from 2005-2013. The differences are expressed as percent of annual mean OLR. Thin white lines are incremented every 2%.

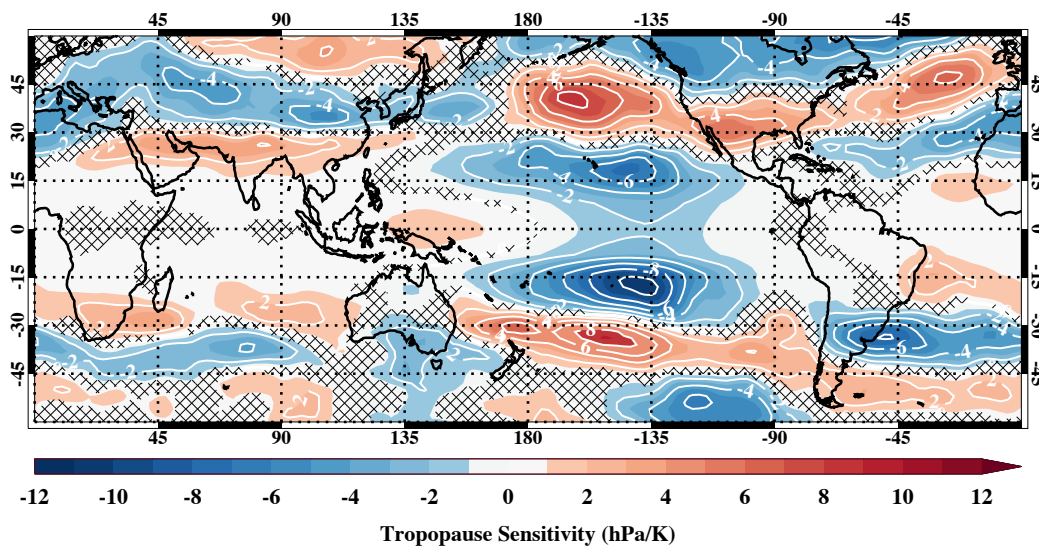


Figure 9. The sensitivity of tropopause pressure to the Niño 3.4 index from linear regression over 2005-2013. The sensitivity is expressed as the change in tropopause pressure per degree change in the index (hPa/K). Crosshatched regions denote where the sensitivity is not statistically different from zero at the 95% confidence level. White contours are incremented every 2 hPa/K.

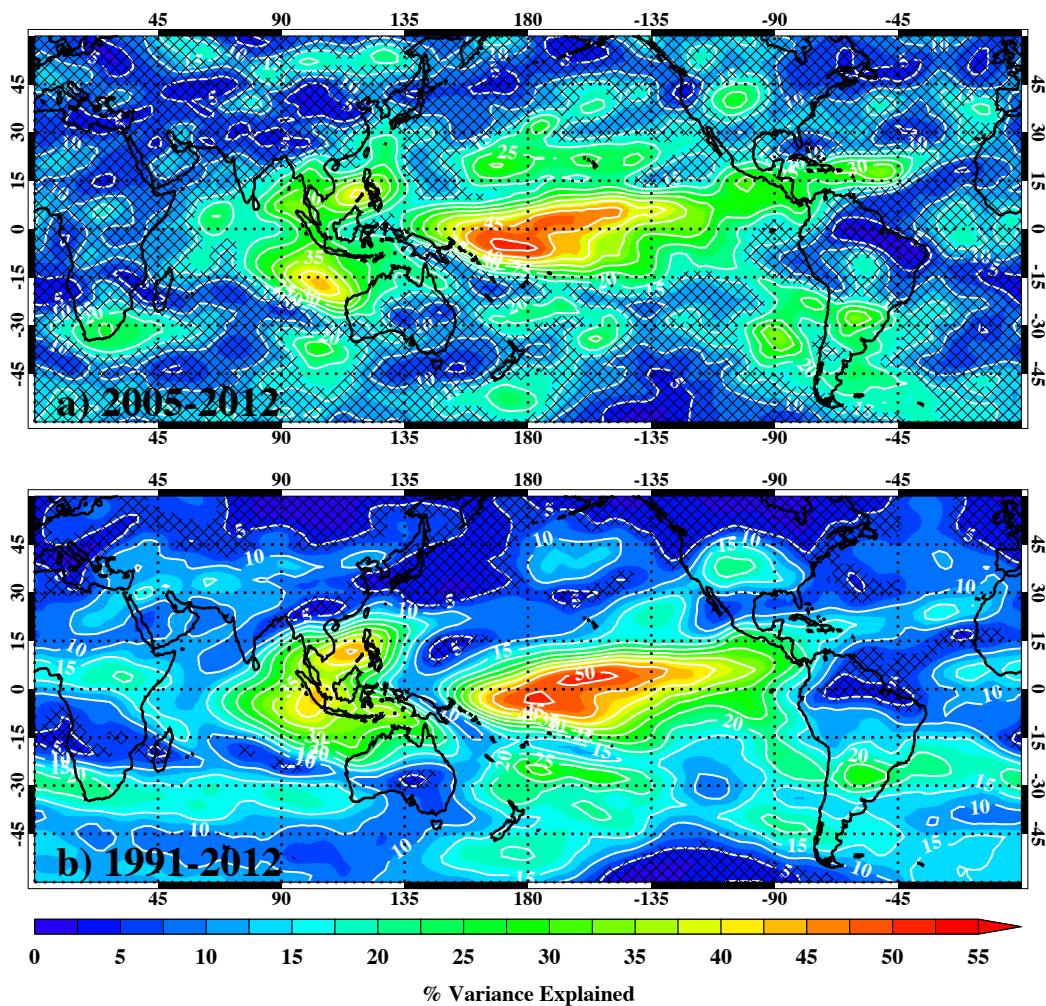


Figure 10. The deseasonalized TCO variance explained by ENSO in the GMI CTM simulation for years (a) 2005-2012 and (b) 1991-2012. Crosshatched areas denote where the confidence level of the explained variance being different from zero is less than 95%. The increment of the white contours is 5%.